PHOTON-COUNTING SOLID-STATE PHOTOMULTIPLIER

M. D. Petroff and M. G. Stapelbroek
Rockwell International Corporation
Science Center
Anaheim, California 92803

ABSTRACT

The solid-state photomultiplier is a silicon device capable of continuous detection of individual photons in the wavelength range from 0.4 to 28 μm. Operated with an applied bias near 7 volts, the device responds to the absorption of an incident photon with a submicrosecond-rise-time current pulse having a narrow amplitude distribution well above the electronic readout noise level. Optimal photon-counting performance occurs between 6 and 10 K and for count rates less than 10^{10} counts/s per cm^2 of detector area. A 60% counting quantum efficiency has been demonstrated at 20 μm, and near 60% was observed in the visible light region. The underlying mechanism involves extremely fast internal charge amplification by impact ionization of impurity-band electrons and results in a pulse for each photoelectrically or thermally induced free carrier. The thermally induced dark pulse rate at 7 K is sufficiently low that background limited detector performance is obtained at a background of less than 10^6 photons/cm^2s.

INTRODUCTION

Solid-state counterparts of the vacuum-tube photomultiplier capable of counting individual photons have been sought for decades following a proposal for a solid state quantum counter by Bloembergen.[1] Some limited photon counting ability has been demonstrated using avalanche photodiodes (APDs) biased above their normal breakdown voltage in a gated mode.[2,3] Other recent attempts to develop solid-state photomultipliers include novel device structures such as those being developed by Capasso and coworkers[4,7] by band-gap engineering of the III-V semiconductor materials.

To our knowledge solid-state photomultiplier (SSPM) developed at Rockwell[8] is the only solid-state device that has demonstrated continuous counting of individual photons. Further, it is the only detector that can count photons of energy much less than one eV with high quantum efficiency. Using arsenic-doped silicon (Si:As) as the detector material, it is based on an extension of the blocked-impurity-band (BIB) detector concept developed earlier at Rockwell.[9] These devices utilize impurity-band conduction (IBC), a phenomenon also called impurity semiconductor hopping conductivity[10]. When such material is doped to sufficiently high concentrations and cooled to carrier freeze-out temperatures holes in the otherwise completely filled impurity band can be treated as mobile carriers on an equal footing with conduction band electrons and valence band holes. For example in the Si:As material of BIB detectors the carriers are conduction band electrons with a mobility of about 10^3 cm^2/Vs and donor impurity band holes (D^+ charges) with a mobility of about one cm^2/Vs. In effect the material can be considered as an intrinsic semiconductor with a band gap energy equal to the impurity ionization energy. The operation of the BIB detector can thus be understood in terms of a reverse-biased impurity-band photodiode. The SSPM, in this view, operates as a very-high-gain avalanche photodiode (APD). However, in contrast to conventional APDs, the SSPM has several unique advantages that derive from the nature of IBC on which the device is based. For the same semiconductor, impurity-band impact ionization occurs at much lower field strengths.

The direct and immediate consequence of detecting a single photon with the SSPM is a current pulse containing from about 2×10^4 to 6×10^4 electrons on average. Even with a very simple amplifier, such pulses are easily seen above amplifier noise. Dispersion in the amplitudes of individual photon pulses is very low in the SSPM because:[8] 1) only one carrier type can impact ionize; 2) the avalanche process is very localized which causes avalanche quenching effects: and 3) since electron scattering in IBC material is largely elastic until impurity ionization energies are reached fairly uniform electron doubling lengths lead to well ordered avalanche growth with distance.

The useful spectral sensitivity of Si:As SSPMs spans the wavelength range between about 0.4 to 28 μm with peaks near 0.5 and 24 μm and a minimum around 1.0 μm. Counting quantum efficiencies of about 0.60 have been measured at both peaks. The counting quantum efficiency is defined as the ratio of countable photon-detection events to the total number of incident photons. Si:As-based SSPMs require operating temperatures between 5 and 10 K. Time resolution is on the order of several nanoseconds for SSPMs, making them useful for applications where timing the arrival of photons is important.

DEVICE STRUCTURE AND OPERATION

Device operation will be discussed in terms of existing n-type structures using arsenic-doped silicon (Si:As). The front-illuminated, single-crystal structure shown in Fig. 1(a) consists of a doped infrared-active layer (IRL) and a thin, undoped blocking layer (BL) grown epitaxially on a silicon

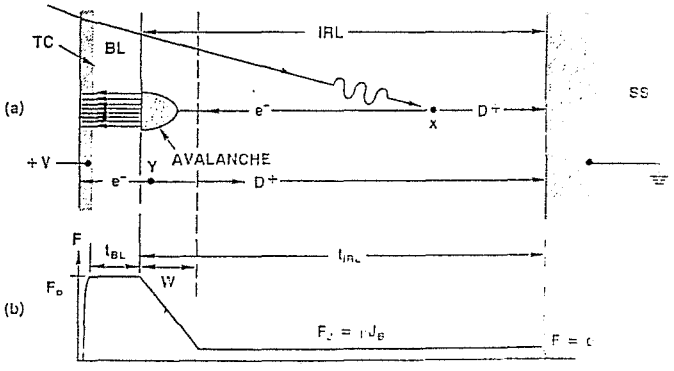

(a) SSPM LAYER CONFIGURATION WITH SCHEMATIC REPRESENTATION OF THE GENERATION OF BIAS CURRENT AND THE EFFECTS FOLLOWING ABSORPTION OF A PHOTON.
(b) ELECTRIC-FIELD PROFILE

Figure 1. SSPM Operating Principle

substrate (SS) doped above the metal-insulator transition.[11] The arsenic concentration in the IRL is about 5 x 10^{17} cm^{-3}, sufficiently high for positively charged impurity-band carriers (D^+ charges) to have a drift mobility on the order of 1 cm^2-V^{-1}-s^{-1}.[12] A controlled acceptor concentration in the range of 5 x 10^{13} to 8 x 10^{14} cm^{-3} is required in the IRL. A transparent contact is formed in the BL by arsenic ion implantation. As illustrated in Fig. 1, this device structure and appropriate bias conditions make possible the creation of localized avalanches in a thin ($\simeq$ 4 μm) high electric field region (gain region) of the device, in response to photon absorption events in a thick ($\simeq$ 25 μm) low field region (drift region).

From charge neutrality, in the absence of an applied electric field, the concentration of D^+ charges is equal to the total acceptor concentration, N_A, all of which are ionized. With the device at a temperature in the range of 6 to 10 K, application of a bias voltage of 7 V establishes the electric field profile shown in Fig 1(b). A constant field, F_o $\simeq$ 7 x 10^3 V-cm^{-1}, will appear in the BL (assumed to be free of any impurities). In the IRL, mobile D^+ charges are depleted away from the BL, leaving negative space charge due to fixed ionized acceptors (A^- charges). As a result, the field decreases linearly with distance into the IRL with a slope equal to $-eN_A/\varepsilon\varepsilon_o$, where e is the magnitude of the electron charge and $\varepsilon\varepsilon_o$ is the permittivity of silicon. The field does not drop to zero at the end of the depletion region[8] since the undepleted part supports an induced field $F_J = \rho J$ due to resistivity ρ ($\simeq$ 10^6 to 10^8 Ω-cm), and a bias current density J generated near the BL via field-assisted thermal ionization (the Poole-Frenkel effect).[13]

An electron-D^+ pair, created by an IR photon (or by thermal generation) at point X in Fig 1(a), is separated by the field F_J. The electron drifts rapidly to the left, with a negligible probability for impact ionization while in the low field region, and the D^+ charge drifts more slowly to the right. An avalanche of well-defined gain, M ($\simeq$ 4 x 10^4 at V = 7 V and T = 7 K), occurs for each electron entering the steeply-increasing electric field region adjacent to the BL. A more complex process involving impact ionization by intrinsically generated holes from the BL entering the IRL is involved for the visible-light response. Holes are very effective in impact ionization of neutral impurities thus initiating an avalanche that differs little from one caused by photoelectron appearing in the low field drift region.

The high and well defined gain obtained in each avalanche is explained by the strong dependence of the impurity impact ionization coefficient on field strength and the limit to avalanche growth due to localized field collapse induced by space charge of the relatively-immobile D^+ charges formed in the avalanche. Collection of the electrons occurs in times on the order of a nanosecond. The achievable gain, M, depends on the field strength and is of the order of $M \simeq A\varepsilon\varepsilon_o F_o/e$, where A is the area over which the avalanche spreads.[12] D^+ charges formed in the avalanche are incapable of ionizing neutral impurities because their energies are restricted to the narrow impurity band. They drift out of the depletion region in less than a microsecond, and enter the undepleted drift layer where their charge is fully dissipated by dielectric relaxation in a time on the order of $\varepsilon\varepsilon_o\rho$. The high impact-ionization gain does not apply to the electron-D^+ pairs responsible for the biasing current, which is generated preferentially in the highest field region close to the BL by field-assisted thermal emission. The electrons from these pairs cannot cause avalanches of large gain. Although the bias current may be larger than the average current due to the SSPM pulses, its contribution to noise is very small because of the small gain.

PHOTON DETECTION AND COUNTING

Data, some of which are presented in this paper, were obtained with Si:As SSPMs with optically-active areas between 0.005 x 0.005 cm^2 and 0.1 x 0.18 cm^2, including ten-element line arrays of 0.01 x 0.025 cm^2 detectors, six by six element area arrays of .015 x .015 cm^2 detectors, 50 x 10 element arrays of .0125 x .0125 cm^2 detectors on .015 cm centers. Test chips with some of the above mentioned detectors and arrays are shown in the photographs of Fig. 2. The

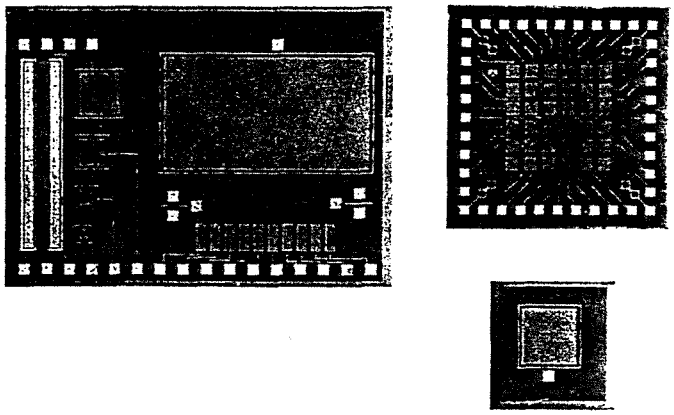

Figure 2. SSPM Test Chips

devices were evaluated in a variable temperature, low-infrared-background, pinhole cryostat represented in Fig. 3. It is equipped with an InAs 3.2 μm wave-length light-emitting diode (LED) located about 10 cm from the SSPM and an optical fiber that permits illumination with visible and near-infrared light from an external source. Radiation passing through the pinhole was attenuated and filtered by a cold bandpass filter. SSPM pulses were observed with simple transimpedance amplifiers (TIAs) external to the dewar followed by further amplification. Typical experimental setup is shown in Fig. 4. The amplified pulses were observed with an oscilloscope and counted or analysed by other instruments.

When operated with a simple amplifier, photogeneration of a single carrier in the SSPM is detected as a submicrosecond-rise-time pulse with an amplitude well above the noise level. The oscilloscope trace of Fig. 5(a) shows the detection of individual photons by a 0.01 x 0.01 cm^2 SSPM for

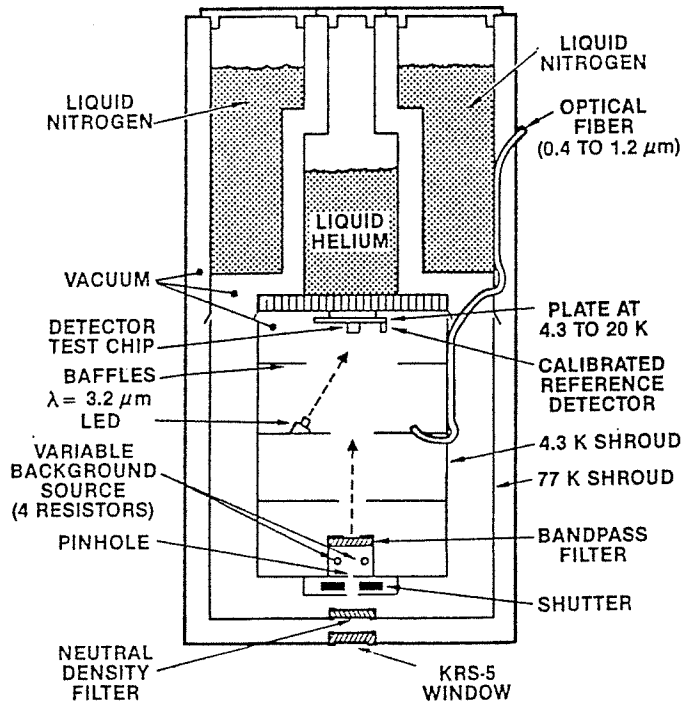

Figure 3. SSPM Test Dewar

an incident photon-flux density of 2 x 10^{8} cm^{-2}-s^{-1} at λ = 20 μm, as measured by a calibrated reference detector. Each pulse has nearly equal amplitude for every photogenerated carrier and is the result of

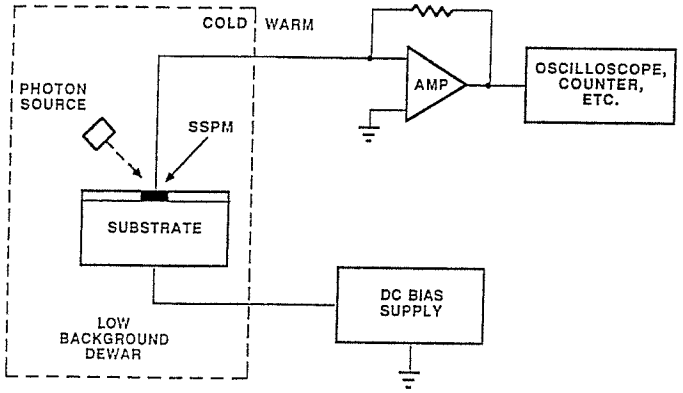

Figure 4. Experimental Setup

extremely fast internal charge amplification by impact ionization of impurity-band electrons as explained in the discussion of the operating principles of the device. The mechanism provides very

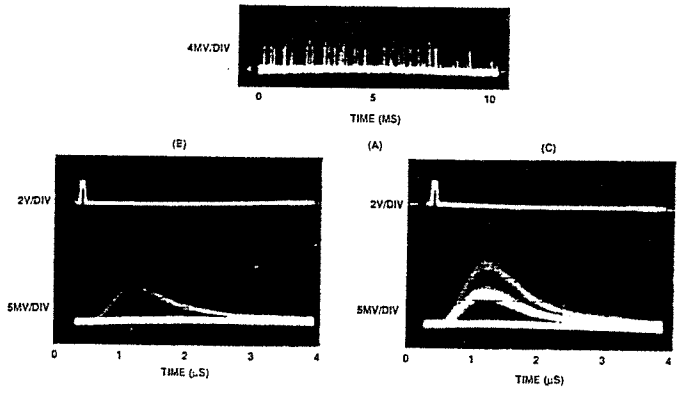

Figure 5. Oscilloscope Traces Showing SSPM Output Pulses

large and uniform carrier multiplication factors in well-localized and self-limiting avalanches. Photons absorbed simultaneously in different parts of the device create separate avalanches whose amplitudes are additive. Larger pulses also occur when two photons are detected within a time less than the amplifier-limited pulse width (amplifier bandwidth is 100 kHz in this case). At T = 7 K and V = 7.5 V about 10% of the pulses are dark pulses, each of which is due to thermal generation of a carrier in the active volume of the device. Dark pulses are indistinguishable from photon pulses and are observed when the pinhole is closed and the photon-flux density inside the cryostat cold chamber is well below the 10^{6} cm^{-2}-s^{-1} measurement limit of the reference detector.

The average pulse rate minus the dark count rate, at a given temperature and bias, is proportional to the average number of incident photons as long as the number of counts per second per unit area is below a temperature-dependent, saturation-count-rate density. Saturation is attributed to a drop of the local electric field in the gain region due to trapping of a small fraction of the avalanche D^{+} charges next to fixed A^{-} sites in the low field region. The affected area is estimated to be about 2 x 10^{-6} cm^{2} from experimental data on the saturation-count-rate density and on the relaxation time of the trapped charge. At T = 7 K, the measured relaxation time is about 50 μs.

A more dramatic demonstration of individual photon detection is provided by the response of the SSPM to very short-duration bursts of λ = 3.2 μm photons generated by the LED, as shown in Figs. 5(b) and 5(c). The top oscilloscope traces in these two photos show short (< 0.1 μs) voltage pulses applied to the LED at a repetition rate of 10,000 s^{-1}. The bottom traces show the resulting superposition of SSPM outputs. In Fig 5(b), the average number of photons detected (deflected traces) per burst from the LED is about 0.2, as determined by a pulse counter. Comparison of intensities between deflected and undeflected traces is consistent with this ratio. (The observed delay between the LED burst and the start of the SSPM pulses and their pulse shape is due entirely to amplifier characteristics.) Figure 5(c) shows the effect of an increase in the number of photons emitted per LED burst so that an average of 1.5 photons per burst is detected. Here, several bands of pulse amplitudes are observed. The first deflected band corresponds to one photon detected per LED burst, the second corresponds to two photons, and the fainter third band of pulses is formed when three photons are detected simultaneously within a fraction of the amplifier time constant. More-quantitative measurements of SSPM pulse amplitudes using a multichannel pulse height analyzer verified that their occurrence rate follows the expected Poisson distribution for randomly-occurring photon absorption events. These data, and similar data using a faster amplifier with 5 MHz bandwidth, conclusively prove that SSPMs are true single-photon detectors with sub-microsecond response to photon incidence.

Several important performance characteristics are presented in Fig. 6 from data obtained on a 0.01 x 0.01 cm^{2} device from the first fabrication lot of SSPMs. Figure 6(a) shows that the dark-count-rate density and the saturation-count-rate density are strong functions of temperature, as expected for

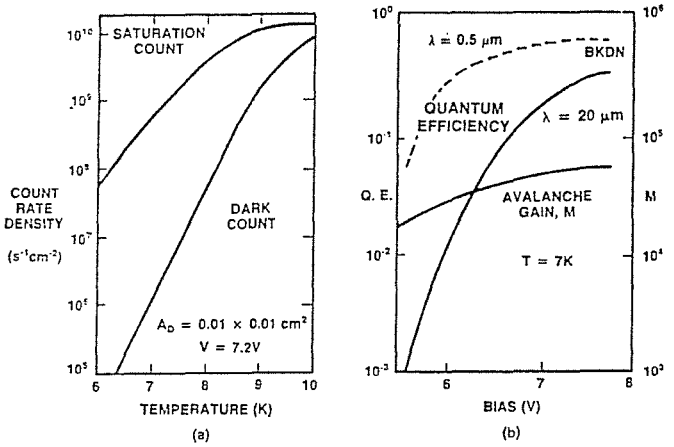

(a) TEMPERATURE DEPENDENCE OF THE SSPM DARK-COUNT-RATE AND SATURATION-COUNT-RATE DENSITIES.
(b) BIAS DEPENDENCE OF GAIN, M, AND QUANTUM EFFICIENCY

Figure 6. SSPM Characteristics

thermally-activated processes. Figure 6(b) gives the measured counting quantum efficiency, η_c, at λ = 20 μm and λ = .5 μm, and gain at a temperature of 7 K as a function of bias. The strong dependence of η_c in the IR response region on applied voltage above 5 V is explained by the pronounced effect of voltage on the ohmic field F_J in the IRL which determines the probability of photo-electrons reaching the gain region[12]. The bias dependence of η_c for visible light is shown in the dashed curve. Here the avalanches are caused by holes generated in the blocking layer. The holes evidently survive in their drift through the gain region while copiously producing electrons by impurity impact ionization. The slow variation of gain with bias is due to the relatively small effect of bias voltage above 5 V on the high electric field in the gain region. From measured values of η_c at λ = 20 μm and the dark-count-rate density, the noise-equivalent power of a 0.01 x 0.01 cm^2 SSPM is estimated to be about 2 x 10^{-19} W-Hz$^{-1/2}$ at T = 6 K and V = 7.25 V. Some of the performance characteristics of Fig. 6 have been exceeded in subsequent fabrication lots. Through design changes suggested by the SSPM operational model the dark count rate at a given temperature has been reduced by about a factor of ten and the long wavelength quantum efficiency has been increased to 0.6 at λ = 20 μm. However, the new devices have a 2 to 3 times wider response pulse amplitude distribution and a lower saturation count rate density. Improvements in these performance characteristics are anticipated in future fabrication lots.

The spectral dependence of η_c in the IR region was measured with band-pass filters (λ = 4.5, 10, 15, 20 μm) and λ = 0.9 and 3.2 μm LEDS calibrated with a reference detector of known spectral response. In the visible-light region, η_c was determined by light from a monochromator calibrated with a silicon photodiode of known spectral quantum efficiency. The observed spectral behavior has been adequately explained in terms of the known intrinsic and extrinsic absorption coefficients of the Si:As material. Obtainable quantum efficiencies depend on how the SSPM is illuminated. The useful spectral sensitivity of Si:As SSPMs spans the wavelength range between about 0.4 to 28 μm with peaks near 0.5 and 24 μm and a minimum around 1.0 μm. The original devices were front illuminated; back-illuminated devices were developed later. For these illumination modes η_c values of about 0.60 have been measured at both peaks with η_c measured higher than 0.04 near the minimum for back-illuminated devices. Edge illumination was successfully implemented for the wavelength region near 1 micrometer allowing an order of magnitude higher values of η_c in this region. Calculation of the spectral quantum efficiency for the three different illumination modes for typical SSPM parameters is shown in Figure 7. The data from recent devices falls close to these curves. The decline in quantum efficiency for long wavelength edge illumination is due to about 25 to 50 μm of inactive material between the polished edge and the detector active volume. This dead region is necessary to prevent excessive surface leakage along the edge. Further increases in quantum efficiency in the short wavelength IR region can be obtained by increasing the thickness of the IR-active layer and, for all wavelengths, by the use of antireflection coatings.

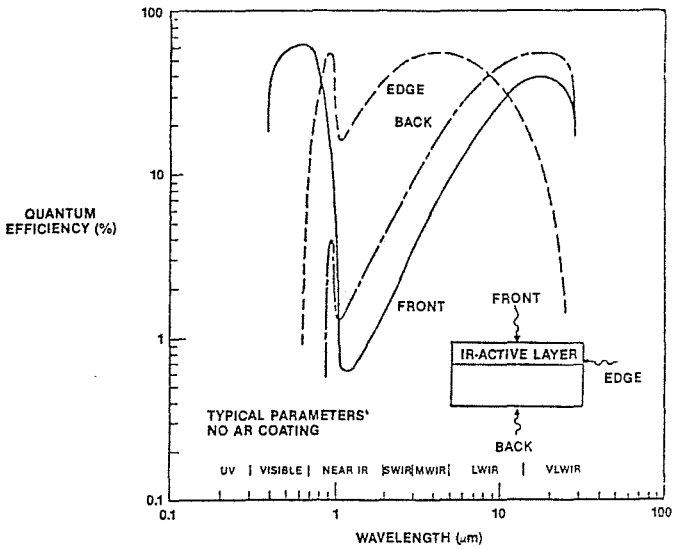

Figure 7. Quantum Efficiency for Different Illumination Modes

CONCLUDING REMARKS

The high quantum efficiency in the entire region between the ultraviolet and the far-infrared and the large and fast gain of the SSPM establish it as the most sensitive photon detector. The noise equivalent power of the SSPM at λ = 20 μm is less than 10^{-19} W/Hz$^{1/2}$ as determined from the dark count rate and quantum efficiency of recently fabricated devices. Obvious applications in the visible light region are wherever photomultipliers or microchannel plates are now being used since the SSPM offers comparable single photon response but with much higher quantum efficiency. Of course, in some applications the liquid helium temperature requirement and use of the necessary cold IR blocking filters may be a disadvantage. SSPMs promise to be especially effective in fiber optic applications in the visible and near IR region. This is because fibers greatly simplify the optical coupling of a device inside a dewar at liquid helium temperatures to the warm outside world. Fibers designed to have a high transmission in the visible and near IR light region are natural cold blockers of the longer wavelength thermal radiation background. One clear application is for detection of visible light photons produced by high energy particles in scintillating fibers.[14]

While SSPMs offer mainly a large quantum efficiency advantage over other photon counters in the visible, the SSPM is unique in the IR wavelength region above 1 μm in that at present no other detectors are capable of counting single photons continuously. But SSPMs will not displace other IR detectors in most applications where background limited operation is already obtainable. Their distinct advantages are in very low background situations, for example in large space IR telescopes, high resolution laser radar ranging, high resolution IR spectroscopy of weak emission lines, and in laboratory experiments and measurements of correlated photon emission events carried out in chambers or dewars where the IR background can be kept low by cryogenic cooling. Particle tracking using IR scintillating fibers is a possibility that needs to be examined since it may allow higher spatial resolution if the photon yield is higher than for visible light fibers.

REFERENCES

[1] N. Bloembergen, Phys. Rev. Lett. 2. 84 (1959).

[2] T. E. Ingerson, R. J. Kearney, and R. L. Coulter, Appl. Opt. 22, 2013 (1983).

[3] B. F. Levine and C. G. Bethea, Appl. Phys. Lett. 44 553 (1984).

[4] F. Capasso, in Semiconductors and Semimetals, edited by R. K. Willardson and A. C. Beer (Academic, New York, 1985), Vol. 22, Part D, p. 2.

[5] F. Capasso, W. T. Tsang, and G. F. Williams, IEEE Trans. Electron Devices ED-30, 381 (1983).

[6] F. Capasso, J. Allam, A. Y. Cho, K. Mohammed, R. J. Malik, A. L. Hutchinson, and D. Sivco, Appl. Phys. Lett. 48, 1294 (1986).

[7] J. Allam, F. Capasso, K. Alavi, and A. Y. Cho, IEEE Electron Device Lett. EDL-8, 4 (1987).

[8] M. D. Petroff, M. G. Stapelbroek, and W. A. Kleinhans, Appl. Phys. Lett. 51, 406 (1987).

[9] M. D. Petroff and M. G. Stapelbroek, U. S. Patent No. 4 568 960 (4 February 1986).

[10] B. I. Shklovskii and A. L. Efros "Electronic Properties of Doped Semiconductors", Springer-Verlag, Berlin (1984).

[11] N. F. Mott and E. A. Davis, Electronic Processes in Non-Crystaline materials (Clarendon, Oxford, 1979).

[12] M. D. Petroff and M. G. Stapelbroek (unpublished).

[13] A. G. Milnes, Deep Impurities in Semiconductors (Wiley, New York, 1973).

[14] M. D. Petroff and M. Atac, "High Energy Particle Tracking Using Scintillating Fibers and Solid State Photomultipliers", IEEE 1988 Nuclear Science Symposium; Orlando, Florida; Nov. 1988.